Flow in oscillatory boundary layers over permeable beds

Claudio Meza-Valle[1] and Nimish Pujara[1]
Department of Civil and Environmental Engineering, University of Wisconsin–Madison, Madison, WI 53706, USA

(*Electronic mail: npujara@wisc.edu)

(Dated: 7 March 2023)

In fluid dynamics applications that involve flow adjacent to a porous medium, there exists some ambiguity in how to model the interface. Despite different developments, there is no agreed upon boundary condition that should be applied at the interface. We present a new analytical solution for laminar boundary layers over permeable beds driven by oscillatory free stream motion where flow in the permeable region follows Darcy's law. We study the fluid boundary layer for two different boundary conditions at the interface between the fluid and a permeable bed that was first introduced in the context of steady flows: a mixed boundary condition proposed in G. S. Beavers and D. D. Joseph, J. Fluid Mech. 30, 197–207 (1967) and the velocity continuity condition proposed in M. Le Bars and M. G. Worster, J. Fluid Mech. 550, 149–173 (2006). Our analytical solution based on the velocity continuity condition agrees very well with numerical results using the mixed boundary condition, suggesting that the simpler velocity boundary condition is able to accurately capture the flow physics near the interface. Further, we compare our solution against experimental data in an oscillatory boundary layer generated by water waves propagating over a permeable bed, and find good agreement. Our results show the existence of a transition zone below the interface, where the boundary layer flow still dominates. The depth of this transition zone scales with the grain diameter of the porous medium and is proportional to an empirical parameter that we fit to the available data.

I. INTRODUCTION

Oscillatory flows are present in a wide variety of problems across different areas of science and engineering. The well-known and classical solution to the boundary layer formed by oscillatory flow above a fixed flat plate was first presented by Stokes [1]. The continued relevance of the classic solution rests on the fact that more complex situations can often be formulated as a modified version of the classical solution; recent examples include flow driven by oscillating boundaries[2], oscillatory pressure-driven flows[3], flow oscillations in a rotating system[4], boundary layer transition[5], and renewed efforts of quantifying sediment transport in oscillatory boundary layers[6–10]. In all these applications, while there is general agreement on boundary layer solutions for impermeable boundaries, the nature of solutions with permeable boundaries differ substantially due to the ambiguities in modeling the boundary conditions at the interface between the free-fluid and the permeable region[11–20].

Previous developments on the physics of boundary layers over permeable beds relate to steady flows[21–39], where the main challenge is setting appropriate boundary conditions at the interface connecting the free fluid and the porous media flow. One of the most studied boundary conditions to model the physics at the interface is the classical study of Beavers and Joseph [21], which states that at the interface, there exist discontinuities between the velocity gradients occurring in the fluid and inside the porous region, which are related via properties of the porous material such as the permeability and a slip coefficient, which depends on the "structure of the permeable material." Le Bars and Worster [30] provided a significant advance on the Beavers and Joseph [21] boundary condition. They showed how the same boundary condition could be adapted to state a continuity between the free fluid velocity and porous media flow (Darcy's velocity) where the matching condition is applied at a certain depth below the interface. This region is then interpreted as a transition zone within the porous region where the free fluid velocity penetrates. This is consistent with physical intuition; since Darcy's flow is an averaged quantity inside the porous region, there should be a minimum distance below the interface before Darcy's law is valid. Therefore, the matching conditions between the fluid velocity and Darcy's velocity must occur at a distance greater than or equal to the averaging length. This insight provides two advantages: (1) it simplifies the interfacial boundary condition for analytical and numerical treatments and (2) it clarifies why previous studies have found the Beavers and Joseph slip coefficient to also be a function of the flow instead of being solely a function of the porous material. Numerical simulations in Le Bars and Worster [30] show that their boundary condition reproduces closely flow obtained from the original condition proposed by Beavers and Joseph [21]. Additionally, only slight differences are found compared to the Darcy-Brinkman formulation[40].

From subsequent studies, it is now established that there does indeed exist a transition layer inside the porous region into which the free fluid flow penetrates and after which the velocity matches its porous media flow value. Several works[27,30,32,33] state that the characteristic length for this transition zone is represented by the squared root of the permeability, but data from experiments and numerical simulations suggest that the grain diameter may be a better characteristic length for this depth[26,29,31,34]. Both numerical simulations and experiments agree, however, that the thickness of the transition layer remains almost invariant for different flow conditions (*e.g.*, Reynolds numbers, flow channel height).

Building on these developments of steady viscous flow over a permeable bed, we present a set of analytical solutions for the laminar boundary layer velocities induced by linear oscillatory flows over a permeable bed. Previous theories on this matter, such as Liu, Davis, and Downing [13] and McClain,

Huang, and Pietrafesa [14], have not explicitly considered the transition zone found in steady flow. We explicitly include a transition zone in our solutions via an empirical parameter and we find that it scales with the grain diameter. For validation, we include comparisons of our theory with numerical solutions of the boundary layer equations and experimental data from Liu, Davis, and Downing [13], both of which show excellent agreement with the analytical solutions. We also include an error analysis to understand the sensitivity of the solution to the empirical parameter and its agreement with experimental data. Our theory, which is much simpler than previous theories, performs much better against data, albeit with an empirical parameter.

From the analytical results, we also see that the slip velocity at the interface and the boundary layer velocity profiles are sensitive to the permeability of the porous material, while the thickness of the transition zone remains almost unaffected for seabeds with similar characteristics. Our novel method can be seen as an extension to the classical boundary layer formulations for an impermeable boundary condition[1,41,42] to model the oscillatory boundary layer flows over the permeable bed.

The remainder of this paper is structured as follows. Section II presents an overview of the oscillatory boundary layer theory, descriptions of different interfacial boundary conditions, and our new analytical solutions. Comparisons with numerical solutions and laboratory data are shown in Section III, where we also include sensitivity and error analysis. Finally, in Section IV we discuss the implications of our work and make concluding remarks.

II. OSCILLATORY BOUNDARY LAYER THEORY

Starting from the classical boundary layer equations[41], we recall the usual assumptions in oscillatory systems that the streamwise length scale is larger than the cross-stream length scale and velocity variations are much stronger in the cross-stream direction than in the streamwise direction. This leads to the neglect of the non-linear advective acceleration in the streamwise momentum equation, which is much smaller than the unsteady acceleration. In dimensionless form, the momentum equations are

$$\frac{\partial u}{\partial t} = \frac{\partial (U\mathrm{e}^{it})}{\partial t} + \frac{\partial^2 u}{\partial \eta^2} \tag{1a}$$

$$0 = \frac{\partial p}{\partial \eta} \tag{1b}$$

where Eq. (1a) and Eq. (1b) correspond to the streamwise and cross-stream momentum balances, respectively, and

$$x = kx' \,; \quad \eta = z'/\sqrt{\nu/\omega} \,; \quad t = \omega t' \,;$$
$$p = p'/\rho U_0^2 \,; \quad (u,w,U) = (u',w',U')/U_0 \tag{2}$$

where x' and z' are the dimensional streamwise and cross-stream coordinates with corresponding dimensional velocities u' and w', respectively. Further, p' is the dynamic fluid pressure, ρ is the fluid density and ν corresponds to the kinematic viscosity of the fluid. The oscillatory free-stream velocity in dimensional form is $U'\mathrm{e}^{i\omega t}$, which has a characteristic magnitude U_0 and where U' is complex and can vary in x'-direction. The cross-stream coordinate z' is scaled by the boundary layer thickness $\sqrt{\nu/\omega}$, and η is therefore the stretched cross-stream coordinate inside the boundary layer. In Eq. (1a), we have used the fact that the free-stream acceleration balances the horizontal pressure gradient

$$-kU_0^2 \frac{\partial p}{\partial x} = \omega U_0 \frac{\partial (U\mathrm{e}^{it})}{\partial t}.$$

The dimensionless continuity equation is

$$\frac{\partial u}{\partial x} + \sqrt{\frac{\omega}{\nu k^2}} \frac{\partial w}{\partial \eta} = 0. \tag{3}$$

where $\sqrt{\omega/\nu k^2}$ is the Womersley number.

We model the flow inside the porous region as described by Darcy's law[43], given in dimensionless form by

$$u_s(x,\eta,t) = -\sigma \frac{U_0}{(\omega/k)} \frac{\partial p}{\partial x} \tag{4}$$

with

$$\sigma = \frac{K\omega}{g} \tag{5}$$

where K is the hydraulic conductivity of the permeable material and g is the gravitational acceleration. σ is the dimensionless hydraulic conductivity.

In what follows, we consider different boundary conditions to model the effects of the porous boundary on the oscillatory boundary layer flow as described by Eqs. (1)-(4).

Interfacial boundary conditions

Working in a two-dimensional Poiseuille flow scenario, Beavers and Joseph [21] (BJ) postulated that there is a transference of the tangent velocity from the fluid to the permeable bed at the interface ($\eta = 0$), which can be treated as a discontinuity between the velocities in these two domains. Physically, at the interface, there is an equilibrium between the velocity gradients above the permeable bed and inside the permeable bed. This boundary condition is written as

$$\frac{\partial u}{\partial \eta} = \frac{\kappa}{\sqrt{\sigma}} (u - u_s) \quad \text{on } \eta = 0. \tag{6}$$

The parameter κ, corresponds to the slip coefficient, and was introduced as an empirical parameter that depends on the structure of the porous material. With κ determined experimentally, BJ's boundary condition yielded good comparison with their experimental data, and the form of their boundary condition was provided further theoretical support by Saffman [22].

Le Bars and Worster [30] (LW) presented an analysis that compared the two-layer system (Stokes flow in the free fluid domain and Darcy's flow in the porous medium) with a single

layer system (Darcy-Brinkman formulation where the porosity smoothly transitions from its porous media value deep within the porous layer to zero in the free fluid). They found that the Stokes flow penetrates to a small depth into the porous medium, which constitutes a transition zone and whose magnitude scales with the pore size. Thus, LW suggest that the BJ boundary condition can be simplified by re-writing it as a continuity between the fluid velocity and Darcy's velocity at a distance δ within the porous boundary

$$u_s = u \quad \text{at } \eta = -\delta \tag{7}$$

where δ is the transition zone depth in dimensionless form. LW further show that this transition depth takes the following form (in our notation)

$$\delta = m\sqrt{\frac{\sigma}{n}} \tag{8}$$

where n is the porosity and m is an $\mathcal{O}(1)$ constant. The equivalence between the LW boundary condition (Eq. (7)) and the BJ boundary condition (Eq. (6)) also showed that $\kappa = \sqrt{n}$, which was consistent with the original postulate that κ was a property of the porous material.

As $\sigma \to 0$, both the BJ and LW boundary conditions tend towards the expected no-slip condition for an impermeable boundary.

Following others who have used the Carman-Kozeny formulation to interpret the thickness of the transition zone in terms of grain diameters, we substitute the Carman-Kozeny expression[44] into Eq. (8) to get

$$\delta\sqrt{\frac{\nu}{\omega}} \approx mD_s\frac{n}{\sqrt{180}(1-n)} \tag{9}$$

where $\delta\sqrt{\nu/\omega}$ on the left side is the dimensional transition zone depth and D_s is the grain diameter of the porous boundary. This shows that the value of the transition depth, which could scale either with the square root of the permeability or with the grain diameter, will be determined by the value of the empirical constant m.

Analytical solutions for LW boundary condition

To consider the LW boundary conditions in the oscillatory flow problem, first we introduce a shifted vertical coordinate that includes the depth of the transition zone in the domain as

$$\bar{\eta} = \eta + \delta. \tag{10}$$

Then, it is possible to state that $u = u_s$ at $\bar{\eta} = 0$, and the LW boundary conditions can be written as

$$u \to U \text{ as } \bar{\eta} \to \infty \tag{11a}$$

$$u = \mathrm{i}\sigma U\mathrm{e}^{\mathrm{i}t} \text{ on } \bar{\eta} = 0. \tag{11b}$$

To find a solution to the governing equation Eq. (1a) subject to boundary conditions Eqs. (11), we assume the solution has a separable form

$$u = \mathbb{R}[f(\bar{\eta})\mathrm{e}^{\mathrm{i}(t+\phi)}] \tag{12}$$

where $\mathbb{R}$ correspond to the real part and ϕ is a phase shift. Substituting Eq. (12) into the governing equation leads to a second order ordinary differential equation with constant coefficients

$$f''(\bar{\eta}) - \mathrm{i}f(\bar{\eta}) = -\mathrm{i}U\mathrm{e}^{-\mathrm{i}\phi} \tag{13}$$

that can be solved with a pair of complex roots and a particular solution $f(\bar{\eta})_p = U\mathrm{e}^{-\mathrm{i}\phi}$. We obtain the following general solution for $f(\bar{\eta})$

$$f(\bar{\eta}) = A\mathrm{e}^{\bar{\eta}\frac{(1+\mathrm{i})}{\sqrt{2}}} + B\mathrm{e}^{-\bar{\eta}\frac{(1+\mathrm{i})}{\sqrt{2}}} + U\mathrm{e}^{-\mathrm{i}\phi}. \tag{14}$$

where A and B are constants to be determined from the boundary conditions in Eqs. (11). $A = 0$ if the solution is to remain finite and satisfy the boundary condition as $\bar{\eta} \to \infty$. B and ϕ are found from the boundary condition at $\bar{\eta} = 0$ to be

$$B = -U\sqrt{1+\sigma^2}$$
$$\phi = -\arctan(\sigma).$$

This final solution is

$$u = U\mathrm{e}^{it}\left[1 - \sqrt{1+\sigma^2}\mathrm{e}^{-\bar{\eta}\frac{(1+\mathrm{i})}{\sqrt{2}}}\mathrm{e}^{-\mathrm{i}\arctan(\sigma)}\right]. \tag{15}$$

The bed shear stress can be computed via

$$\tau_b = \left.\frac{\partial u}{\partial \eta}\right|_{\eta=0}$$

which is given by

$$\tau_b = \sqrt{\frac{1+\sigma^2}{2}}\mathrm{e}^{-\mathrm{i}\arctan(\sigma)}(1+\mathrm{i})\mathrm{e}^{-\delta\frac{(1+\mathrm{i})}{\sqrt{2}}}U\mathrm{e}^{it}. \tag{16}$$

The vertical velocity in the boundary layer can be computed from continuity. Rearranging Eq. (3) gives

$$w - w_s = -\sqrt{\frac{\nu k^2}{\omega}}\int_{-\delta}^{\eta}\frac{\partial u}{\partial x}d\eta$$

where we have used the LW boundary condition to ensure continuity of the fluid and Darcy velocities at the transition depth: $w = w_s$ at $\eta = -\delta$. Here, $w_s = 0$ since $\partial p/\partial\eta = 0$, and the solution for the vertical velocity is

$$w = -\frac{dU}{dx}\sqrt{\frac{\nu k^2}{\omega}}\mathrm{e}^{it}\left\{\bar{\eta} + \sqrt{\frac{1+\sigma^2}{2}}\mathrm{e}^{-\mathrm{i}\arctan(\sigma)}(1-\mathrm{i})\left[\mathrm{e}^{-\bar{\eta}\frac{(1+\mathrm{i})}{\sqrt{2}}} - 1\right]\right\}. \tag{17}$$

The set of solutions for the horizontal velocity, vertical velocity, and bed shear stress (Eq. (15)–(17)) are extensions of the well-known the Stokes boundary layer with a permeable bed. Indeed, as the hydraulic conductivity vanishes $\sigma \to 0$, we recover the classical solutions[1,41,45].

III. NUMERICAL SOLUTIONS AND LABORATORY EXPERIMENTS

In this section, we demonstrate the validity of our analytical solutions by comparing them against numerical solutions and data from laboratory experiments.

A. Numerical solutions

We solve the governing equation for the horizontal velocity in the boundary layer (Eq. (1a)) numerically using finite differences and the Crank-Nicolson semi-implicit scheme. We use the BJ boundary condition at $\eta = 0$ and initialize the simulations with $u(\bar{\eta},0) = 0$. The vertical coordinate η is discretized over a range from 0 to 10 and time is discretized such that $\Delta t/(\Delta\eta)^2 = 0.5$. We simulate the solution for three oscillation cycles from $t = -4\pi$ to 2π and find that the solution reaches its period steady state value within the first two cycles allowing comparisons against the analytical solution to be made in the time span $0 < t < 2\pi$.

The numerical implementation of the Crank-Nicolson scheme to discretize the governing equation (Eq. (1a)) in time (n) and space (j) is presented below. The discretized equation is

$$\frac{u_j^{n+1}-u_j^n}{\Delta t} = \frac{1}{2}\left[\frac{u_{j-1}^{n+1}-2u_j^{n+1}+u_{j+1}^{n+1}}{\Delta\eta^2}\right]+\frac{1}{2}\left[\frac{u_{j-1}^{n}-2u_j^{n+1}+u_{j+1}^{n}}{\Delta\eta^2}\right] + \frac{C_j^{n+1}-C_j^n}{\Delta t} \quad (18)$$

where $C = U\mathrm{e}^{\mathrm{i}t}$ and $\beta = \Delta t/\Delta\eta^2$ corresponds to CFL number. Re-arranging terms leads to the following form

$$-\frac{1}{2}\beta u_{j-1}^{n+1}+(1+\beta)u_j^{n+1}-\frac{1}{2}\beta u_{j+1}^{n+1}-C_j^{n+1} = \frac{1}{2}\beta u_{j-1}^{n}+(1-\beta)u_j^{n}+\frac{1}{2}\beta u_{j+1}^{n}-C_j^{n}. \quad (19)$$

To include the BJ boundary condition (Eq. (6)) in the Eq. (19), which mathematically corresponds to a Robin-type boundary condition, we consider a second order discretization to avoid loss of accuracy. To do this, we make use of a ghost point at the border of the numerical domain. The implementation of LW boundary condition follows a trivial procedure, as it corresponds to a Dirichlet-type boundary condition. The discretization of the BJ boundary condition at time step n is as follows

$$\frac{u_{j-1}^n-u_{j+1}^n}{2\Delta\eta} = \lambda(u_{j+1}^n-u_{s_j}^n) \quad (20)$$

with $\lambda = \kappa/\sqrt{\sigma}$. Re-arranging the above equation, we get the following expression

$$u_{j-1}^n = u_{j+1}^n - 2\Delta\eta[\lambda(u_{j+1}^n-u_{s_j}^n)]. \quad (21)$$

For sake of simplicity, we have skipped the expressions for time step $n+1$ as it is analogous to the aforementioned discretization. Including the boundary terms in Eq. (19), the Crank-Nicolson scheme takes the following form

$$(1+\beta)u_j^{n+1}-\beta u_{j+1}^{n+1} = (1-\beta)u_j^n+\beta u_{j+1}^n-\beta\Delta\eta\lambda(u_{j+1}^{n+1}+u_{j+1}^n)+\beta\Delta\eta\lambda(u_{s_j}^{n+1}+u_{s_j}^n) + (C_j^{n+1}-C_j^n). \quad (22)$$

This is a matrix equation with a tridiagonal matrix, which is easily solved (*e.g.*, using the Thomas algorithm).

To validate our numerical solutions, we checked that the numerical procedure accurately reproduces the classical Stokes boundary layer velocities for a solid impermeable boundary.

In Fig. (1) we show the boundary layer velocity profiles for a permeable bed at different phases of an oscillation cycle. The analytical velocity profiles obtained with the LW boundary conditions (solid magenta) show very good agreement with the numerical solutions with the BJ boundary condition (black dashed line).

To compare the numerical solution with the analytical solution close to the interface $\eta = 0$, we show the time series of slip velocities and bed shear stresses in Fig. (2). From this figure, we again observe an agreement between the analytical and numerical solutions considering LW and BJ boundary conditions, respectively, but also observe small differences. These differences can be attributed to the precise value of the constant m that effectively sets the thickness of the transition zone until the flow is well described by Darcy's law.

In Fig. (3) we show how flow at the interface varies with the dimensionless permeability σ. The maximum value of the slip velocity is shown in panel (a), the maximum bed shear stress value in panel (b), with their respective phase lags in panels (c) and (d). As permeability increases, the slip velocity magnitude increases and the bed shear stress magnitude decreases since the flow encounters lower resistance. The phase lags are less sensitive to the permeability compared with the magnitudes.

B. Comparisons with laboratory data

We compare our analytical solutions against experimental data reported in Liu, Davis, and Downing [13]. In the experiments, surface gravity waves propagate over a permeable bed generating an oscillatory boundary layer The experimental cases are listed in Table I, which gives values for the water depth h, wave amplitude a, wave period T, the dimensionless hydraulic conductivity σ measured using a constant-head permeator, the porosity n, and the dimensionless wave steepness ka and dimensionless wavelength kh calculated using the wavenumber k from the dispersion relation. From linear wave theory, the dimensionless free-stream velocity that drives the boundary layer is given by

$$U = \frac{ka}{\sinh kh}\mathrm{e}^{-\mathrm{i}(x-t)}.$$

This wave-induced flow can be considered to be uniform inside the boundary layer and the flow in the permeable bed (below the transition zone) can be considered to be well modelled by Darcy's law. Thus, the experimental conditions are ideally suited to test our analytical solutions, which can be found by substituting $U = \mathrm{e}^{-\mathrm{i}x}$ into Eq. (15)–(17). The horizontal velocity solution is given by

$$u = U_0\left\{\cos(x-t)-\sqrt{1+\sigma^2}\cos\left(x-t+\frac{\eta+\delta}{\sqrt{2}}+\arctan(\sigma)\right)\mathrm{e}^{-\frac{\eta+\delta}{\sqrt{2}}}\right\} \quad (23)$$

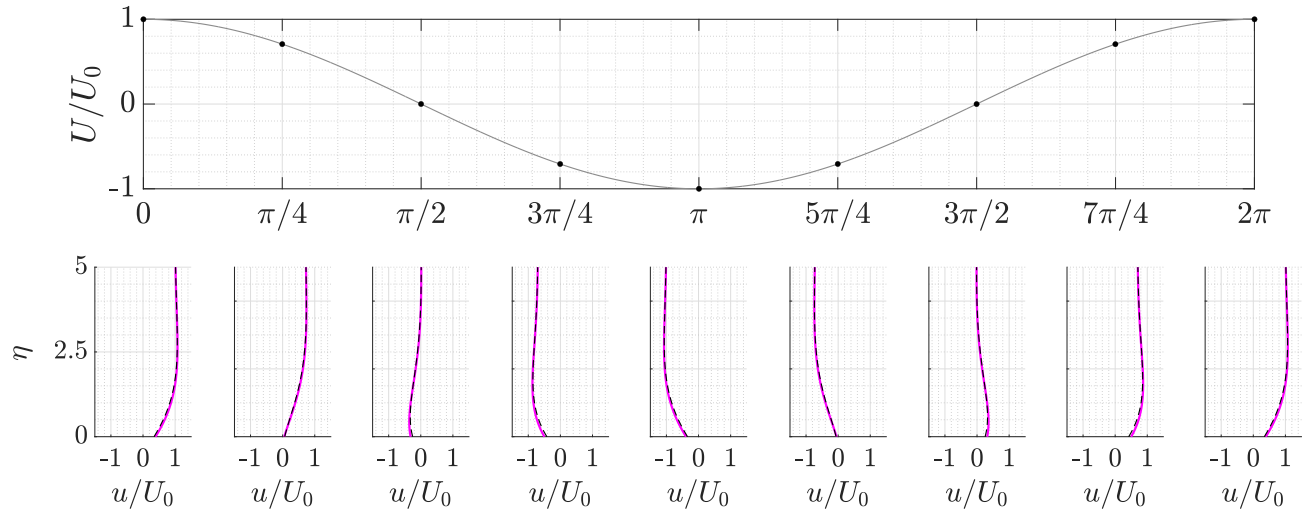

FIG. 1: Velocity profiles for a permeable bed condition for $\sigma = 0.1$ and $U_0 = 1$, and $m = 1$. Top: Free-stream velocity. Bottom: LW boundary condition (analytical solution: solid magenta line), BJ boundary condition (numerical solution: black dashed line).

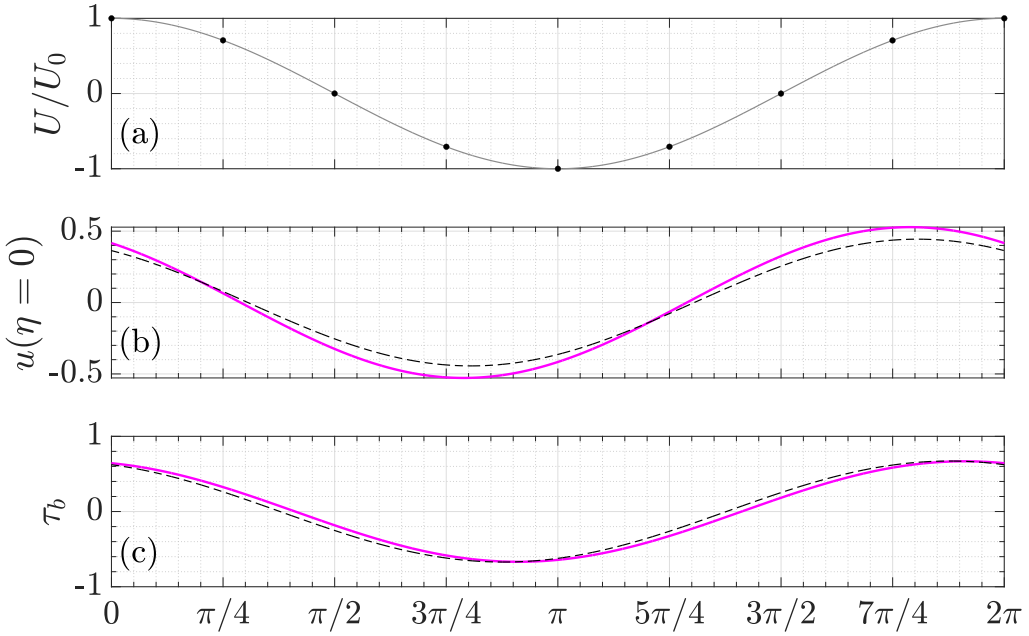

FIG. 2: Slip velocity and shear stress at the interface ($\eta = 0$) for $\sigma = 0.1$ and $U_0 = 1$. a) Free-stream velocity; b) slip velocity; c) Wall shear stress. LW boundary condition analytical solution (solid magenta line), BJ boundary conditionnumerical solution (black dashed line).

where

$$U_0 = \frac{ka}{\sinh kh}.$$

As before, the above expression reduces to the expected impermeable bed solution[42] as $\sigma \to 0$.

Fig. 4 shows the comparison between the analytical solution and experimental data. Here, the parameter m plays an important role because it determines the depth of the transition zone below the interface and essentially controls the magnitude of the slip velocity. Rather than tuning the value of m for each experimental case, we show the comparisons by taking a single value of m for the experiments where the porous medium presents the same characteristics in permeability and porosity (groups 2, 3, and 4). The agreement between the data and our theory is remarkable, especially given that a more detailed matched asymptotic solution in Liu, Davis, and Downing [13] was much less successful.

In order to extend the analysis, we quantify the error considering the averaged Root Mean Squared Error (RMSE) across the experimental cases of groups 2, 3, and 4 shown in Fig. (4).

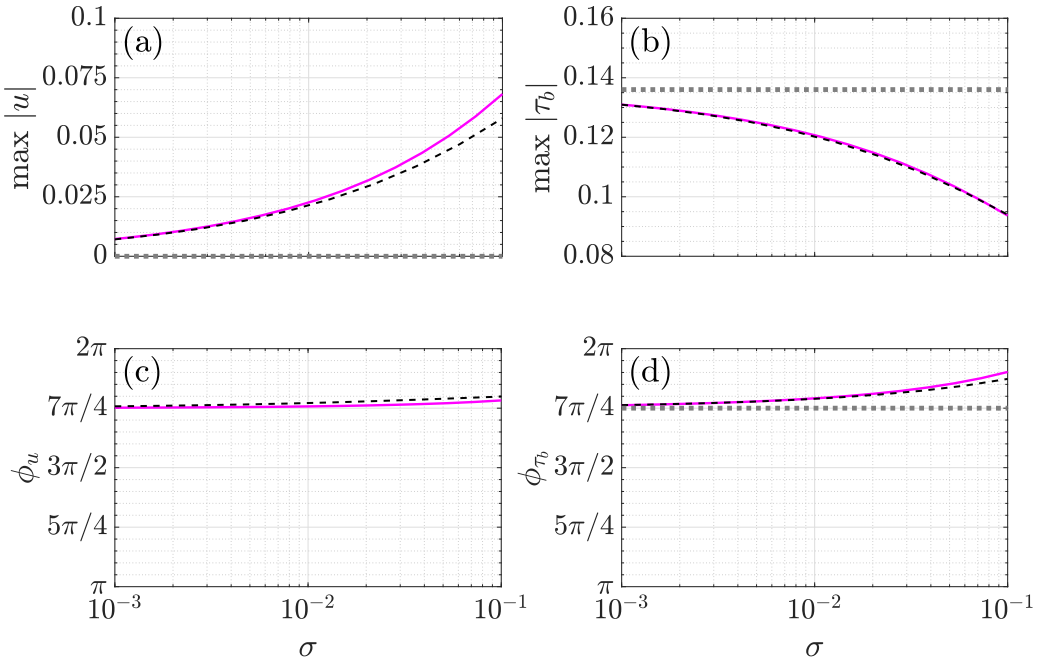

FIG. 3: Top: Variation of the maximum slip velocity (a) and bed shear stress (b) as functions of σ, with $U_0 = 1$. Bottom: Variation of the phase associated to the maximum slip velocity (c) and bed shear stress (d) for different values of σ. Grey line: No-slip boundary condition (analytical solution). Magenta line: LW boundary condition (analytical solution with m = 1). Black dashed line: BJ boundary condition (numerical solution).

TABLE I: Experimental data from Liu, Davis, and Downing [13].

Group	Exp.	$D_s \times 10^{-3}(m)$	a (cm)	h (cm)	T (s)	σ	n	ka	kh
2	A2	0.5	0.517	19.9	1.254	0.0012	0.3830	0.0203	0.7801
3	A3	1.5	0.512	19.9	1.254	0.0090	0.3824	0.0201	0.7801
4	A4	3.0	0.515	19.9	1.254	0.0373	0.3840	0.0202	0.7801
2	B2	0.5	0.537	24.0	1.114	0.0013	0.3830	0.0227	1.0141
3	B3	1.5	0.513	24.0	1.114	0.0102	0.3824	0.0217	1.0141
4	B4	3.0	0.522	24.0	1.116	0.0419	0.3840	0.0220	1.0117
2	C2	0.5	1.181	24.7	1.035	0.0014	0.3830	0.0545	1.1396
3	C3	1.5	1.167	24.7	1.033	0.0109	0.3824	0.0540	1.1426
4	C4	3.0	1.140	24.7	1.035	0.0452	0.3840	0.0526	1.1396

From the analysis, we find the optimum value of m, for which the error is minimum. From Figs. (5a, 5b and 5c) it is possible to visualize the performance of the matching condition of our theory compared to the experiments for different values of the parameter m. In general, the errors associated with the selected values of m for each group are lower compared with the literature.

From Eqs. (8) and (9), we see that the thickness of the transition zone is proportional to both $\sqrt{\sigma}$ or D_s. From the empirical data, we found that a value of $m = 14, 7$ and 4 gives good agreement across different groups of oscillatory flow conditions and permeable beds, and thus, the transition zone thickness remains almost invariant for different oscillatory flow conditions. In terms of the grain diameter it is

$$\delta\sqrt{\frac{\nu}{\omega}} = [0.69, 0.32, 0.19]D_s, \tag{24}$$

and in terms of the permeability it is

$$\delta = [22.62, 11.32, 6.45]\sqrt{\sigma}. \tag{25}$$

The above expressions show different orders of magnitude when the different scales apply, which agrees with previous data[26,33,34]. Since the scaling with grain diameter is closer to a value of 1 than the scaling with the permeability, we interpret our results as suggesting the grain diameter to be a more suitable characteristic length for the transition zone. Different from other studies, we reach this conclusion indirectly by using the empirical parameter m in relation to the boundary layer in the free fluid.

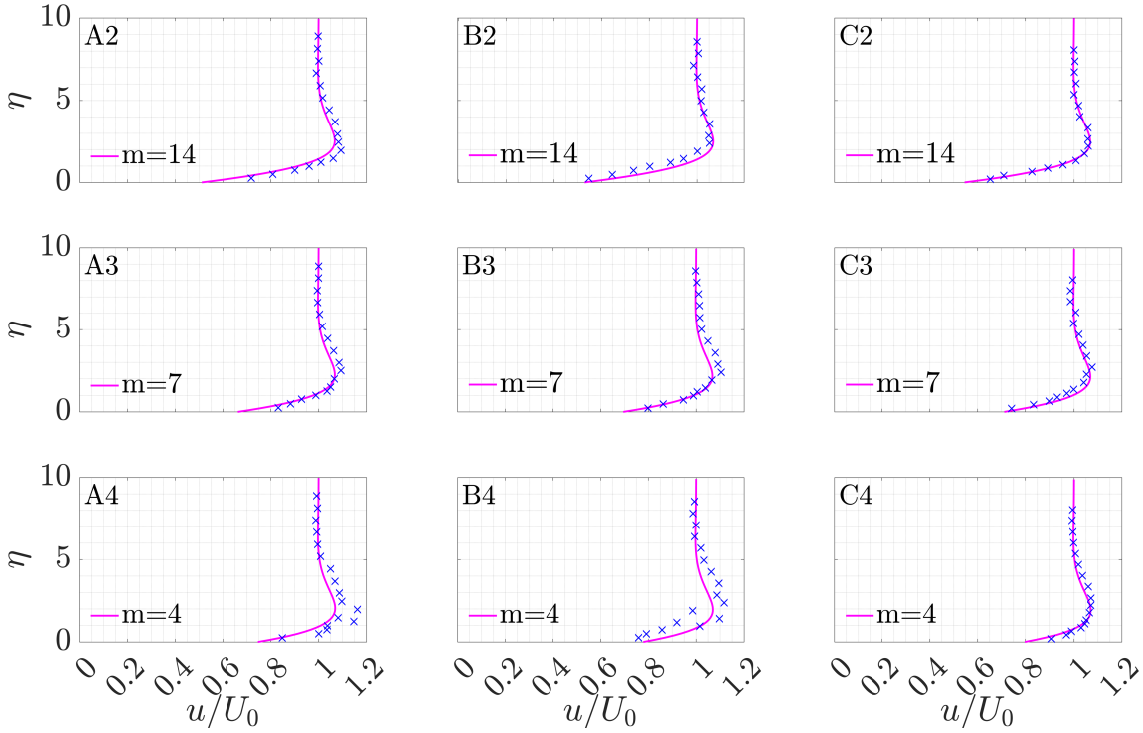

FIG. 4: Dimensionless velocity profiles at $x-t=2\pi$ (under the wave crest) for the different cases listed in Table I, showing a comparison between the LW analytical solution (solid magenta line) and experimental data[13](blue crosses). Labels A2-C4 refer to experimental cases in Table I.

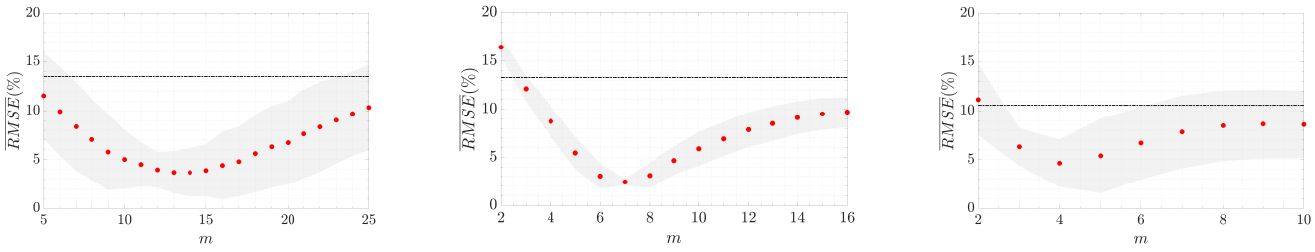

FIG. 5: Average RMSE of velocity magnitudes for different values of m (red dots) compared to Liu et al. (1996) theoretical solution (black dash-dotted line). Errors calculated on experimental data. (a) Group 2; (b) Group 3; (c) Group 4.

IV. CONCLUSIONS

We have found analytical solutions for oscillatory boundary layers over a permeable bed and compared these with numerical solutions and experimental data. The boundary conditions at the interface between the fluid and permeable bed represent the biggest source of uncertainty in such a scenario. In numerical simulations, we apply the well-known Beavers and Joseph[21] boundary condition in our numerical solutions, which states that the velocity gradient above and below the interface is related via a "slip coefficient" that depends on the nature of the permeable bed. For our analytical solutions, we apply the boundary condition discussed in Le Bars and Worster[30], which is closely related to the Beavers and Joseph formulation, but with certain advantages. Our analytical solutions show how the boundary layer structure depends on the dimensionless hydraulic conductivity $\sigma = K\omega/g$, with the solutions recovering the well-known impermeable bed Stokes boundary layer in the limit $\sigma \to 0$. Further, these solutions agree well with numerical solutions in terms of the velocity profiles, slip velocities, and wall shear stresses. The solutions also agree well with experimental data of an oscillatory boundary layer driven by surface waves propagating over a bed of solid spheres. The analytical solutions contain an $\mathcal{O}(1)$ empirical parameter, whose value is constrained with the use of experimental data. We show that, physically, this parameter controls the thickness of the transition zone below which

the flow dynamics are dominated by Darcy's law. Our results broadly agree with previous literature on steady flows that the transition zone thickness is on the order of 1 grain diameter.

The main difference between our approach and past efforts lies in the nature of the interfacial boundary condition. While previous efforts[13,14] use various matching conditions between the free fluid and porous media flow at the interface, our formulation takes into account how the free-fluid flow penetrates slightly into the permeable bed within a transition zone as well-established from work on steady flows. This approach appears to be more effective than introducing a boundary layer based on Darcy's law on the porous medium side of the interface.

We anticipate that future work could extend the physical insights from our results to various applications in coastal engineering and oceanography such as water wave damping[11,46–48], mass exchange, and sediment transport in both laminar and turbulent conditions[49–51], and wave-driven canopy flows[52–54].

ACKNOWLEDGMENTS

We acknowledge support from the U.S. National Science Foundation (grant number OCE-2048676). We also acknowledge anonymous comments from two reviewers.

REFERENCES

[1] G. G. Stokes, *Mathematical and Physical Papers, Volume I.* (Cambridge University Press, 1880).
[2] S. Hossain and N. E. Daidzic, "The shear-driven fluid motion using oscillating boundaries," J. Fluids Eng. **134(5): 051203**, 1–13 (2012).
[3] L. Issa, "A simplified model for unsteady pressure driven flows in circular microchannels of variable cross-section," Appl. Math. Model. **59**, 410–426 (2018).
[4] Y. Song and M. J. Rau, "Viscous fluid flow inside an oscillating cylinder and its extension to stokes' second problem," Phys. Fluids **32, 043601** (2020).
[5] P. Blondeaux and G. Vittori, "Revisiting the momentary stability analysis of the stokes boundary layer," J. Fluid. Mech. **919**, A36:1–15 (2021).
[6] A. Mathieu, Z. Cheng, J. Chauchat, C. Bonamy, and T.-J. Hsu, "Numerical investigation of unsteady effects in oscillatory sheet flows," J. Fluid. Mech. **943**, A7:1–33 (2022).
[7] G. Vittori, P. Blondeaux, M. Mazzuoli, J. Simeonov, and J. Calantoni, "Numerical investigation of unsteady effects in oscillatory sheet flows," Int. J. Multiphase Flow **133**, 1–16 (2020).
[8] M. Mazzuoli, A. G. Kidanemariam, and M. Uhlmann, "Direct numerical simulations of ripples in an oscillatory flow," J. Fluid Mech. **863**, 572–600 (2019).
[9] M. Mazzuoli, P. Blondeaux, G. Vittori, M. Uhlmann, J. Simeonov, and J. Calantoni, "Interface-resolved direct numerical simulations of sediment transport in a turbulent oscillatory boundary layer," J. Fluid Mech. **885**, A28: 1–31 (2020).
[10] G. Fromant, D. Hurther, J. van der Zanden, D. A. van der A, I. Cáceres, T. O'Donoghue, and J. S. Ribberink, "Wave boundary layer hydrodynamics and sheet flow properties under large-scale plunging-type breaking waves," J. Geophys. Res. Oceans **124**, 75–98 (2019).
[11] J. A. Putnam, "Loss of wave energy due to percolation in a permeable sea bottom," Trans. Am. Geophys. Union **30**, 349–356 (1949).
[12] J. N. Hunt, "On the damping of gravity waves propagated over a permeable surface," J. Geophys. Res. **64**, 4:43779–442 (1959).
[13] P. L.-F. Liu, M. Davis, and S. Downing, "Wave–induced boundary layer flows above and in a permeable bed," J. Fluid Mech. **325**, 195–218 (1996).
[14] C. R. McClain, N. E. Huang, and L. J. Pietrafesa, "Application of a 'radiation-type' boundary condition to the wave porous bed problem," J. Phys. Oceanogr. **7:6**, 823–835 (1977).
[15] M. Minale, "Momentum transfer within a porous medium. ii. stress boundary condition," Phys. Fluids **26**, 123102: 1–15 (2014).
[16] J. J. Feng and Y.-N. Young, "Boundary conditions at a gel-fluid interface," Phys. Rev. Fluids **5**, 124304: 1–13 (2020).
[17] A. Samanta, "Role of slip on the linear stability of a liquid flow through a porous channel," Phys. Fluids **29**, 094103: 1–14 (2017).
[18] S. Karmakar, R. Usha, G. Chattopadhyay, S. Millet, J. V. R. Redy, and P. Shukla, "Stability of a plane poiseuille flow in achannel bounded by anisotropic porouswalls," Phys. Fluids **34**, 034103: 1–28 (2022).
[19] L. Li, J. Zhang, Z. Xu, Y.-N. Young, J. J. Feng, and P. Yue, "An arbitrary lagrangian-eulerian method for simulating interfacial dynamics between a hydrogel and a fluid," J. Comput. Phys. **451**, 1–22 (2022).
[20] P. Angot, B. Goyeau, and J. A. Ochoa-Tapia, "A nonlinear asymptotic model for the inertial flow at a fluid-porous interface," Adv. Water Resour. **149**, 1–11 (2021).
[21] G. S. Beavers and D. D. Joseph, "Boundary conditions at a naturally permeable bed," J. Fluid Mech. **30**, 197–207 (1967).
[22] P. G. Saffman, "On the boundary condition at the surface of a porous medium," Stud. Appl. Maths **L(2)**, 93–101 (1971).
[23] J. A. Ochoa-Tapia and S. Whitaker, "Momentum transfer at the boundary between a porous medium and a homogeneous fluid—i. theoretical development," Int. J. Heat Mass Transf. **38**, 2635–2646 (1995).
[24] J. A. Ochoa-Tapia and S. Whitaker, "Momentum transfer at the boundary between a porous medium and a homogeneous fluid—ii. comparison with experiment," Int. J. Heat Mass Transf. **38**, 2647–2655 (1995).
[25] D. F. James and A. M. J. Davis, "Flow at the interface of a model fibrous porous medium," J. Fluid Mech. **426**, 47–72 (2001).
[26] A. Goharzadeh, A. Khalili, and B. B. Jørgensen, "Transition layer thickness at a fluid-porous interface," Phys. Fluids **17**, 057102:1–11 (2005).
[27] N. Tilton and L. Cortalezzi, "Linear stability analysis of pressure-driven flows in channels with porous walls," J. Fluid Mech. **604**, 411–445 (2008).
[28] M. Ghisalberti, "Obstructed shear flows: similarities across systems and scales," J. Fluid Mech. **641**, 51–61 (2009).
[29] B. Goyeau, D. Lhuillier, D. Gobin, and M. Velarde, "The effect of a transition layer between a fluid and a porous medium: shear flow in a channel," Int. J. Heat Mass Transf. **46**, 4071–4081 (2003).
[30] M. Le Bars and M. G. Worster, "Interfacial conditions between a pure fluid and a porous medium: implications for binary alloy solidification," J. Fluid Mech. **550**, 149–173 (2006).
[31] Q. Zhang and A. Prosperetti, "Pressure-driven flow in a two-dimensional channel with porous walls," J. Fluid Mech. **631**, 1–21 (2009).
[32] D. A. Nield, "The beavers–joseph boundary condition and related matters: A historical and critical note," Transp. Porous Med. **78**, 537–540 (2009).
[33] M. R. Morad and A. Khalili, "Transition layer thickness in a fluid-porous medium of multi-sized spherical beads," Exp. Fluids **46**, 323–330 (2009).
[34] Q. Liu and A. Prosperetti, "Pressure-driven flow in a channel with porous walls," J. Fluid Mech. **679**, 77–100 (2011).
[35] S. K. Gupte and S. G. Adavani, "Flow near the permeable boundary of a porous medium: An experimental investigation using lda," Exp. Fluids **22**, 408–422 (1997).
[36] B. Alazmi and K. Vafai, "Analysis of fuid fow and heat transfer interfacial conditions between a porous medium and a fuid layer," Int. J. Heat Mass Transf. **44**, 1375–1749 (2001).
[37] A. Wu and P. Mirbod, "Experimental analysis of the flow near the boundary of random porous media," Phys. Fluids **30**, 047103 (2018).
[38] A. M. Davis and D. F. James, "Penetration of shear flow into an array of rods aligned with the flow," Can J Chem Eng. **82**, 1169–1174 (2004).
[39] J. K. Arthur, D. W. Ruth, and M. F. Tachie, "Porous medium flow and an overlying parallel flow: Piv interrogation area and overlaps, interfacial location, and depth ratio effects," Transp. Porous Media **97**, 5–23 (2013).
[40] H. C. Brinkman, "A calculation of the viscous force exerted by a flowing fluid on a dense swarm of particles," Appl. Sci. Res. **1**, 27–34 (1949).
[41] G. K. Batchelor, *An introduction to Fluid Dynamics* (Cambridge University Press, 2000).

[42]I. A. Svendsen, *Introduction to Nearshore Hydrodynamics* (Advanced Series on Ocean Engineering, 2006).
[43]J. Bear, *Dynamics of Fluids in Porous Media* (Dover, 1972).
[44]P. C. Carman, "Fluid flow through granular beds," Transactions, Institution of Chemical Engineers, London **15**, 150–166 (1937).
[45]L. Rosenhead, *Laminar Boundary Layers* (Dover, 1988).
[46]R. O. Reid and K. Kajiura, "On the damping of gravity waves over a permeable sea bed," Trans. Am. Geophys. Union **38**, 662–666 (1957).
[47]P. L.-F. Liu, "Damping of water waves over porous bed," Journal of the Hydraulics Division **99**, 2263–2271 (1973).
[48]P. L.-F. Liu and R. A. Dalrymple, "The damping of gravity water-waves due to percolation," Coast. Eng. **8**, 33–49 (1984).
[49]P. L.-F. Liu, "Mass transport in water waves propagated over a permeable bed," Coast. Eng. **1**, 79–96 (1977).
[50]D. C. Conley and D. L. Inman, "Ventilated oscillatory boundary layers," J. Fluid Mech. **273**, 261–284 (1994).
[51]S. Corvaro, E. Seta, A. Mancinelli, and M. Brocchini, "Flow dynamics on a porous medium," Coast. Eng. **91**, 280–298 (2014).
[52]M. Luhar, S. Coutu, E. Infantes, S. Fox, and H. Nepf, "Wave-induced velocities inside a model seagrass bed," J. Geophys. Res. **115**, C12005:1–15 (2010).
[53]J.-J. Webber and H.-E. Huppert, "Stokes drift in coral reefs with depth-varying permeability," Philos. Trans. R. Soc. Lond., A **378**, 1–12 (2020).
[54]J.-J. Webber and H.-E. Huppert, "Stokes drift through corals," Environmental Fluid Mechanics **2**, 1–17 (2021).